Available online at www.sciencedirect.com
SCIENCE DIRECT®
International Journal of Heat and Fluid Flow 25 (2004) 702–710
International Journal of HEAT AND FLUID FLOW
www.elsevier.com/locate/ijhff

Full-field velocity and temperature measurements using magnetic resonance imaging in turbulent complex internal flows

C.J. Elkins [a,*], M. Markl [b], A. Iyengar [c], R. Wicker [c], J.K. Eaton [a]

[a] Department of Mechanical Engineering, Stanford University, Stanford, CA 94305, USA
[b] Department of Radiology, Lucas MRI/S Center, Stanford University, Stanford, CA 94305, USA
[c] Mechanical and Industrial Engineering Department, University of Texas at El Paso, El Paso, TX 79968, USA

Received 23 January 2004; accepted 21 May 2004

Abstract

Flow and heat transfer in complex internal passages are difficult to predict due to the presence of strong secondary flows and multiple regions of separation. Two methods based on magnetic resonance imaging called 4D magnetic resonance velocimetry (4D-MRV) and thermometry (4D-MRT) are described for measuring the full-field mean velocities and temperatures, respectively, in complex internal passage flows. 4D-MRV measurements are presented for flow through a model of a gas turbine blade internal cooling passage geometry with $Re_h = 10{,}000$ and compared to PIV measurements in a highly complex 180° bend. Measured three-component velocities provide excellent qualitative and quantitative insight into flow structures throughout the entire flow domain. The velocities agree within ±10% in magnitude and ±10° in direction in a large portion of the bend which is characterized by turbulent fluctuations as high as 10–20% of the passage inlet bulk velocity. Integrated average flow rates are accurate to 4% throughout the flow domain. Preliminary 4D-MRV/MRT results are presented for heated fully developed turbulent pipe flow at $Re_D = 13{,}000$.

1. Introduction

Complex internal flow passages such as those found in heat exchangers, piping manifolds, and turbine cooling passages are difficult to design when there is a target heat transfer rate or pressure distribution. Flows through these passages are highly turbulent with strong secondary flows and multiple regions of separation, and the heat transfer rate can be difficult to predict. Engineers rely on computational fluid dynamics (CFD) in designing these passages, but the flows are extremely difficult to compute. CFD has difficulty predicting multiple regions of separation and even more difficulty predicting the heat transfer through the non-equilibrium boundary layers. Because detailed information is unavailable, designers use large safety factors and rely on analysis based on simple models developed for idealized geometries and boundary conditions. This is especially true for heat transfer. Because of the lack of good analysis tools, several iterations may be required to design a turbine blade with sufficient internal cooling to prevent thermal failure. These design cycles are expensive and time consuming. Designers would like an experimental technique capable of measuring the flow and heat transfer in real internal passage geometries. Such a measurement technique should allow relatively rapid construction of the experiment and data acquisition in order to fit into modern design cycles.

Traditional experimental techniques such as laser Doppler anemometry (LDA) and stereoscopic and/or holographic particle image velocimetry (PIV) can potentially provide detailed flow velocity data. However, these measurements are very difficult if not impossible in most internal passages due to optical access difficulties. Heat transfer measurements are difficult as well. Local

* Corresponding author.
E-mail address: elkins@vonkarman.stanford.edu (C.J. Elkins).

0142-727X/$ - see front matter © 2004 Elsevier Inc. All rights reserved.
doi:10.1016/j.ijheatfluidflow.2004.05.017

temperature measurement requires complex and time consuming installation, and in the end does not provide the full-field heat transfer information designers require. Of course, full-field measurements are virtually impossible to make with traditional techniques.

Magnetic resonance velocimetry (MRV) and thermometry (MRT) present alternative methods for non-invasively obtaining full-field velocity and temperature data in complex internal flows. MRV and MRT are based on the same principles used in magnetic resonance imaging (MRI), now applied routinely in the medical field. In this paper, we employ a technique called 4D magnetic resonance velocimetry (4D-MRV) to non-invasively measure the full three-dimensional mean velocity field in a complex turbulent internal flow. We assess the accuracy of MRV by taking PIV measurements in the same flow. Finally, we evaluate the potential of the same 4D-MRV technique for making both velocity and temperature measurements in fully developed heated pipe flow.

Fukushima (1999) and Mantle and Sederman (2003) detail several MRI fluid mechanics studies many of which apply to low Reynolds number multiphase flows or laminar pulsatile physiologic flows. Turbulent studies include flow through straight pipes (Li et al., 1994; Gatenby and Gore, 1996) and through stenotic (partially obstructed) pipes (Ku et al., 1990; Oshinski et al., 1995; Seigel et al., 1996; Gach and Lowe, 2000). Most of these studies measured velocities in 2D planes through the flow. At present, 3D or 4D (three spatial dimensions and time) techniques (Markl et al., 2002; Bogren and Buonocore, 1999; Ebbers et al., 2001; Kozerke et al., 2001) provide the capability of obtaining the mean flow field in complex 3D volumes in very reasonable amounts of time. Elkins et al. (2003) detail the use of phase-contrast 4D-MRV in a gas turbine blade internal cooling geometry similar to the one presented here. These measurements demonstrated the effectiveness of 4D-MRV in turbulent flows.

MRI systems have also been used to measure temperature in tissues (Cline et al., 1996; Bertsch et al., 1998; Diedrich et al., 2001), in food processing systems (Nott and Hall, 1999) and recently in laminar flows (Ogawa et al., 2000; Sun and Hall, 2001). These studies utilize one or combinations of three methods for measuring temperature with MRI. These methods are based on the temperature dependence of the diffusion coefficient, the spin lattice relaxation time (T_1), and the proton resonant frequency (sometimes referred to as chemical shift). The temperature dependence of the resonant frequency arises from changes in hydrogen bonds, exhibiting a strong effect in water. We hypothesized that the phase-contrast 4D-MRV sequence of Markl et al. (2002) could be used to measure temperature in addition to velocity. This can be accomplished if the phase changes due to the temperature dependent proton resonant frequency shift can be measured in the presence of velocity induced phase changes.

The purpose of this paper is threefold. First, we present full-field measurements of the three-component mean velocity field acquired using the 4D-MRV technique in a model gas turbine blade cooling passage. Sample measurements are shown here illustrating selected flow features. Full results are available on our web site. Second, we present PIV measurements and compare them with the MRV results to evaluate the accuracy of the technique. The final objective is to evaluate the potential use of the 4D-MRV technique for providing full-field temperature measurements in a turbulent flow. Experiments were conducted in a heated pipe flow to assess the accuracy of the temperature measurements in a turbulent flow.

2. Methods

2.1. Flow models

Three-component mean velocity data were acquired in a simplified model of the internal cooling passages used in gas turbine blades. These serpentine passages include sharp bends and angled ribs (also called turbulators) attached to two of the four channel walls. Fig. 1 shows the model with a few of its important dimensions. The model includes angled ribs of square cross section and three bends with varied shapes. The inlet and outlet are converging and diverging nozzles, respectively. Each has a circular cross section of diameter 3.49 cm that contorts into the square cross section (2.0 cm by 2.0 cm) of the passage over a distance of 3.0 cm. These nozzles facilitate the use of fully developed pipe flow for inlet flow conditions to provide a well-defined initial condition for use in comparing CFD results.

The model was drawn using SolidWorks and made out of RenShape^{TM} 5220 stereolithography (SL) resin with a 3D Systems 250/50 SL machine in less than 24 h. There are several advantages to using SL models. First, the model can be made very quickly with an arbitrarily complex internal flow geometry. The challenge is designing internal flow geometries such that the SL machine can fabricate the model without the use of internal support structures that would otherwise require access for removal. Second, SL produces very accurate models. The present model was built with a layer resolution of 0.10 mm, providing an accurate rendition of the geometry and a smooth finish on the internal surfaces. Third, SL models are compatible with MRI systems, unlike metal models, as long as the water absorption of the resin is low. If the appropriate resin is used, there are very few model-related artifacts in the MRI images. Last, the SL model of the internal passage is somewhat transparent (there are several MRI-compatible transparent

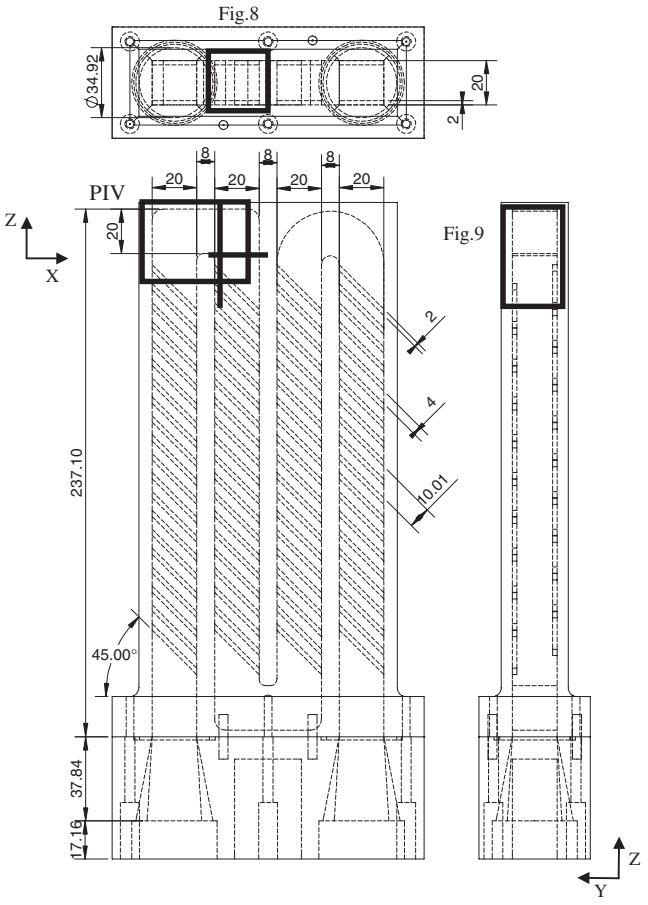

Fig. 1. Drawing of the internal passage model (units = mm). Note the outlined regions indicate regions shown in Figs. 4–9. The labels indicate the corresponding figure number.

materials available), allowing visual inspection of the internal passages. This is especially useful when filling the model with water and purging bubbles from the system.

A second identical SL internal passage model was manufactured and modified to allow optical access for PIV measurements. Two surfaces in the region of the first bend were machined and replaced with glass windows. One window (2.5 cm by 3.8 cm) was placed on the end of the first passage of the model to allow for laser sheet access. The second window (5.3 cm by 3.0 cm) was placed on a sidewall so that illuminated particle images could be captured using the PIV camera. The region of PIV interrogation is shown in Fig. 1.

A 2.3 m long rigid, straight, acrylic pipe with 3.18 cm ID was used as the flow model for the MRV/MRT experiment in which fully developed, heated and unheated isothermal pipe flow was measured. The acrylic pipe had a 3.2 mm wall thickness and was assumed to be a good insulator which limited the heat loss along its length.

2.2. MR system and sequence

Magnetic resonance imaging (MRI) is a technique for generating spatially resolved images inside an object utilizing static and gradient magnetic fields and radio frequency (RF) pulses. Most medical MRI machines, including the one used for this investigation, image hydrogen nuclei (spinning protons). For a discussion of the principles of MRI, the reader is referred to Stark and Bradley (1999), von Schulthess and Hennig (1998), and Haacke et al. (1999). In addition, a brief discussion of MRV principles is found in Elkins et al. (2003) where the 4D-MRV technique is described in detail.

All measurements were performed on a 1.5 T system (Signa CV/i, GE, G_{max}=40 mT/m, rise time = 268 μs). Images were acquired using a standard head coil for all experiments. This is a receiving coil normally used for imaging a patient's head. Using this smaller receiving coil provides higher signal to noise ratio measurements than using the standard receiving coil (body coil) built into the MRI machine.

The 3D volume including the internal cooling passage model shown in Fig. 1 was scanned with a slab thickness of 36 mm and a field of view (FOV) of 280 mm resulting in a volume with dimension $36 \times 280 \times 280$ mm. An imaging matrix of $36 \times 256 \times 256$ resulted in a pixel resolution of $1.0 \times 1.09 \times 1.09$ mm. The sequence parameters were TE = 1.9 ms, TR = 5.9 ms, $n_{kz} = 6$, flip angle = 15° with a Venc factor of 250 cm/s in all directions. In each case, six complete data sets were acquired in a period of 27 min. The six data sets were averaged to reduce noise.

The 3D volume around the heated turbulent pipe flow was scanned with a slab thickness of 48 mm and FOV of 260 mm by 65 mm. The imaging matrix was $48 \times 256 \times 64$ which gave a pixel resolution of 1.0 mm × 1.02 mm × 1.02 mm. Sequence parameters were TE = 5.7 ms, TR = 11.7 ms, $n_{kz} = 2$, flip angle = 15° and a Venc of 90 cm/s in all directions. Flow and temperature measurements required three independent scans each with different flow and temperature: (1) unheated stationary flow, (2) unheated fully developed turbulent flow, and (3) heated fully developed turbulent flow. To compute the velocity, the phase image from the 1st scan was subtracted from the 2nd scan and the resulting phase was converted to velocity by multiplying by Venc/π. The temperature was calculated by subtracting the 2nd scan phase image from the 3rd scan phase image and converting the phase difference to temperature difference using the formula

$$dT = d\phi \Big/ \left(2\pi \frac{df}{dT} TE\right)$$

where dT is the temperature difference, $d\phi$ is the measured phase difference, and df/dT is the change in spin resonant frequency with temperature (≈0.64 Hz/°C in the 1.5 T system).

2.3. Internal cooling passage steady flow loop

Both the MRV and PIV experiments used similar steady flow loops. The MRV steady flow loop was set up using a centrifugal pump (Little Giant model no. TE-6MD-HC) to circulate water. Gadolinium-based contrast agent (Omniscan, Nycomed, Inc.) was added in a concentration of 0.5%. The average flow was measured using the bucket and stopwatch method with an estimated uncertainty of 5%. The flow rate was 10 L/min. The cross sectional area of the passage inlet is 4 cm^2, so the mean bulk passage inlet velocity is 41.7 cm/s. MRV places a few restrictions on the experimental setup due to the large magnetic field and the sensitivity to RF noise. The pump was placed approximately 3 m from the magnet, and no other metallic parts were used in the loop. The Little Giant pump was tested for RF interference and was found to produce a minimal amount of noise in MR images.

After traveling approximately 2 m through 2.54 cm ID flexible tubing, the fluid entered a 2.3 m long rigid, straight, transparent polycarbonate pipe with 3.49 cm ID to produce fully developed turbulent pipe flow ($Re_D = 7000$) at the inlet to the model. The Reynolds number through the model was $Re_h = 10{,}000$, where h is the passage height (2.0 cm).

2.4. Heated pipe steady flow loop

This experiment used the same pump and fluid as described in Section 2.3. The fluid traveled approximately 2 m through 2.54 cm ID flexible tubing before entering the rigid acrylic pipe. Fully developed, isothermal pipe flow was measured near the end of this pipe.

A circulating immersion heater (Cole-Parmer model 12105-30) in the supply reservoir raised the fluid temperature 30 °C above the unheated case. Three different flow and temperature conditions were created: (1) stationary flow at 26 °C, (2) fully developed turbulent flow at 26 °C and $Re_D = 13{,}000$, and (3) heated fully developed turbulent flow at 56 °C and $Re_D = 23{,}000$. The volumetric flow rate was measured with the bucket and stopwatch method to be 17.7 L/min. The heated and unheated flows had the same volumetric flow rates, and it is assumed that the velocity fields were the same although the Reynolds numbers were different. The plastic pipe was assumed to be highly insulating so that the temperature profile in the fluid was isothermal and the same temperature as the supply reservoir.

2.5. PIV system

The PIV system consisted of a commercially available camera, synchronizer, and software from TSI, Inc., and a laser from NewWave Research. To form a light sheet, a −15 mm focal length concave lens and a 500 mm spherical lens were mounted directly on the head of the NewWave Research Gemini 532 nm, 200 mJ PIV Nd:YAG laser. Due to space restrictions, the laser was mounted normal to the light sheet window so a mirror (Newport 20QM20HM.35) was required to redirect the light into the test section. A 12 bit, 1.3 megapixel camera with 1280×1024 pixel format (TSI PIVCAM 13-8) was used for the experiments. The camera was mounted on a unislide assembly (Velmex A40) to a fixed rail above the test section and faced vertically downward.

A custom calibration target was manufactured using SL (3D Systems Viper si2 rapid prototyping machine with DSM Somos WaterShed resin) to fit within the model passage and bend at the mid-plane of the flow passage. The target was painted with flat black spray paint and an array of holes was filled with white silicone. This procedure has been used effectively for various geometries. In the present case, a simple pixel ratio calibration (of 32.1 μm/pixel) was sufficient for the entire illuminated region.

Polyamide seeding particles from Dantec Inc. with a mean diameter of 20 μm, diameter range between 5 and 35 μm, and density of 1.03 g/cc were used to seed the flow. Approximately 2 teaspoons of particles per 5 gallons of distilled water were used. The flow loop for PIV incorporated a temperature control system that maintained the fluid at 23 °C within ±0.5 °C.

One thousand image pairs were processed using Insight (TSI, Inc.) incorporating a bilinear peak search algorithm in a two frame cross correlation with the Hart engine. Full field images were used for analysis with no image shift or spot offset, and pixel spacing between the vectors was 16×16 with a 32×32 interrogation window. This yielded vectors with spacing of 0.50 mm in the physical domain so that every other vector (with 1.03 mm spacing) could be used for comparison with the MRV results. Each vector within the instantaneous vector fields was validated once using a 3 standard deviation criterion. The estimated uncertainty of the mean velocity measurements is ±4.0% for the majority of the flow except near the walls.

3. Results

3.1. Internal passage velocity measurements

Fig. 2 shows 4D-MRV signal magnitude images for an image plane at approximately the mid-height of the ribs on one of the passage walls. Note that the turbulators are well resolved. Comparing the image with flow to the flow-off image gives an idea of the effect of flow on the signal magnitude. In the flow-off image, the signal magnitude is nearly uniform except, of course, inside the turbulators where there are no water molecules. In regions of high velocity fluctuations, the magnitude

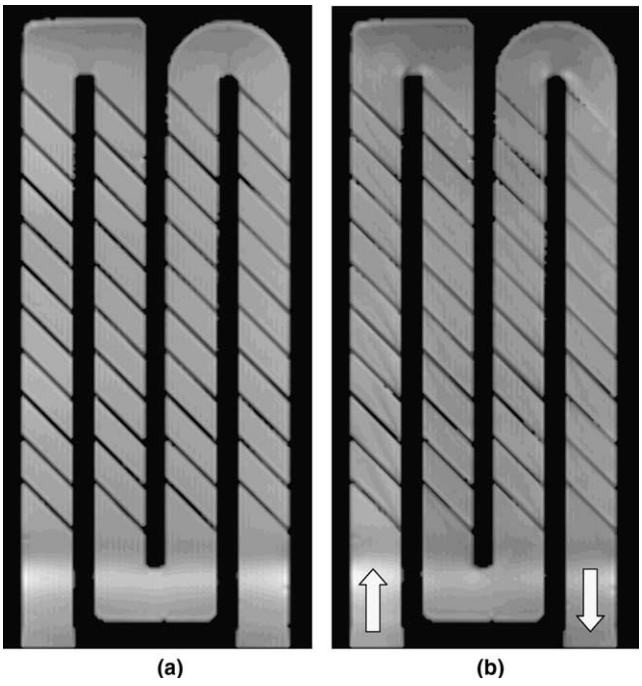

Fig. 2. Magnitude images created from the 4D-MRV sequence for flow off (a) and flow on conditions for $Re_h = 10{,}000$ (b). Increasing brightness corresponds to increasing signal magnitude. Both images show slice planes through the half height of the turbulators. Note that the turbulators are well resolved. Flow features behind the turbulators are evident in dark streaks. Arrows indicate flow direction.

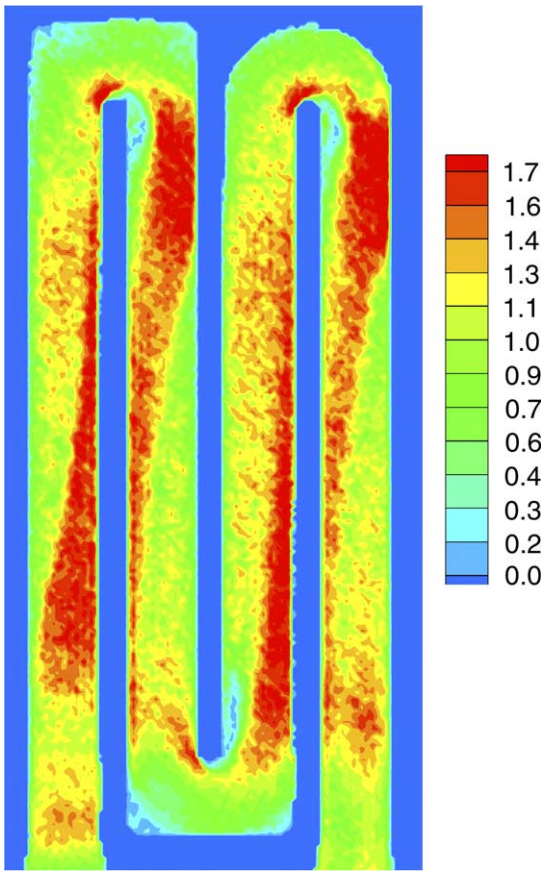

Fig. 3. Contour plot of the normalized velocity magnitude in the center plane of the internal passage flow domain.

decreases because the turbulence causes dephasing of the signal in that region. This is seen in the reattachment lines behind the turbulators. Fig. 3 shows the velocity magnitude contours in the center plane of the entire model to illustrate that MRV captures mean velocities for the whole flow domain.

As a test of the accuracy of the mean velocity measurements, the average flow rate was calculated by integrating the measured velocity profiles at several cross sections in the model and averaging. The value of 9.6 L/min agreed to within the uncertainty of the value measured with the bucket and stopwatch method (10 L/min ± 5%).

The PIV measurements of the center plane in the first bend are compared to the MRV measurements in the vector plot shown in Fig. 4. To allow direct comparison, the MRV results were interpolated onto the PIV grid since both methods produced data with similar resolution. The region shown is a slightly enlarged area from the acquired field of view of the PIV. The vectors compare very well in magnitude and direction throughout the flow including the separation region downstream of the bend. Both measurement techniques show the flow converging just upstream of the bend, nearly horizontal flow at the bend, and flow separation after the bend with the same size recirculation zone.

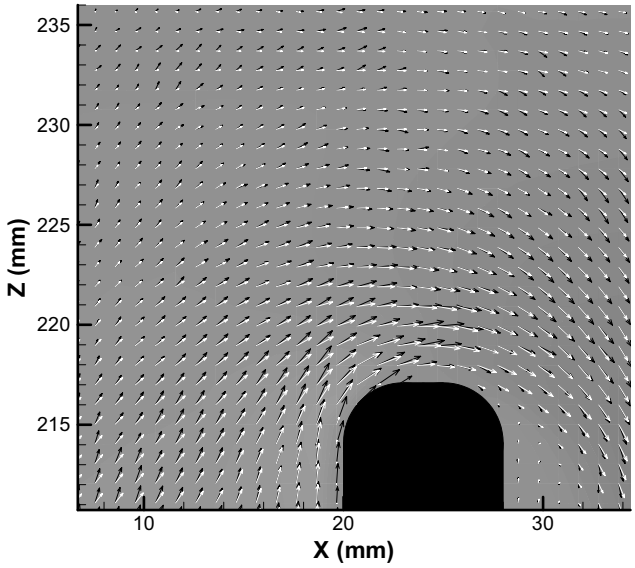

Fig. 4. Comparison between mean velocity vectors from PIV (white) and MRV (black) in the center plane of the first bend.

Fig. 5 shows the magnitude of the velocity fluctuation (measured using PIV) normalized by the passage inlet

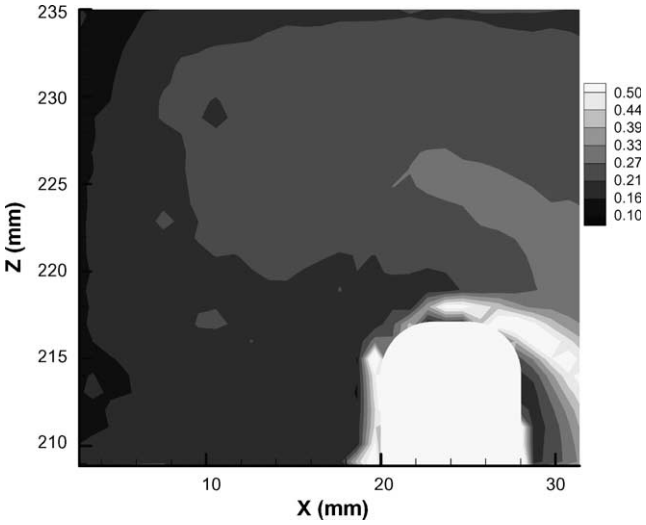

Fig. 5. The magnitude of the velocity fluctuation normalized by the passage inlet bulk velocity.

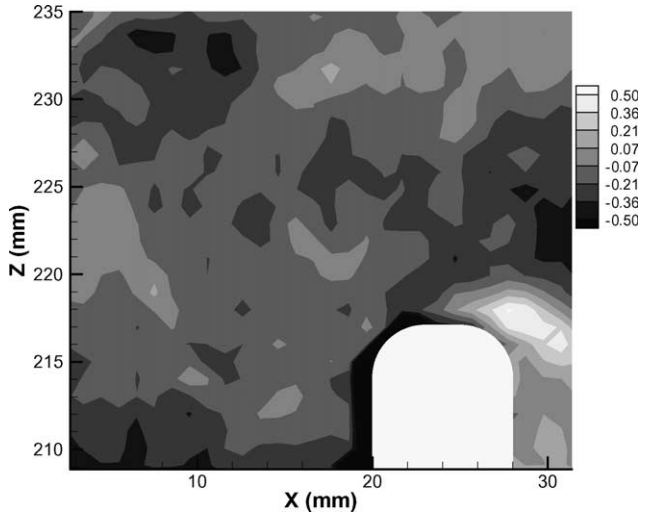

Fig. 6. The PIV velocity magnitude minus the MRV magnitude normalized by the passage inlet bulk velocity.

bulk velocity. Figs. 5–7 show the same region of the flow which is slightly larger than the region in Fig. 4. The velocity fluctuations are quite high (approximately 10–20% of the passage inlet bulk velocity) throughout the flow in the bend, and the shear layer around the downstream separation region has very high velocity fluctuations (greater than 40% of the inlet bulk velocity). Figs. 6 and 7 show the errors between the PIV and MRV velocity magnitudes and angles, respectively. Fig. 4 shows that the high speed regions of the flow are close to the bend. In this area, the MRV measures velocities within ±10% of the PIV while errors in the shear layer around the separation region are as high as 40%. The angle measured with MRV is predominantly within ±10°. Errors are higher in the shear layer of the separation region where the fluctuations are large.

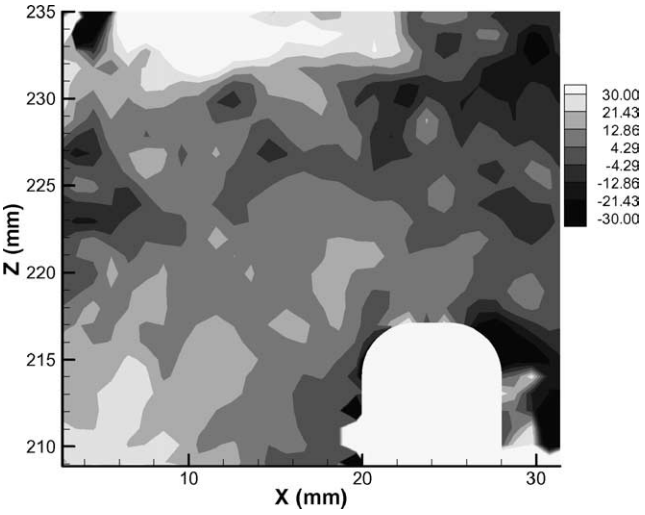

Fig. 7. The MRV velocity angle minus the PIV angle in degrees. Positive angle is counterclockwise from the X axis.

The MRV data cover the complete 3D domain of the flow model shown in Fig. 1. With such a large amount of data, it is difficult to present all of the interesting features of the flow field. To illustrate the detail available, data from the two additional planes in the region around the first bend are presented in Figs. 8 and 9. The positions of these planes are shown in Fig. 1. The complete data set is available from the authors on their website.

Fig. 8 shows a view of the flow in the second passage at the level of the bend. Note the presence of secondary flow structures. In particular, there is a pair of corner vortices and a stagnation region at the right hand wall in the middle of the channel.

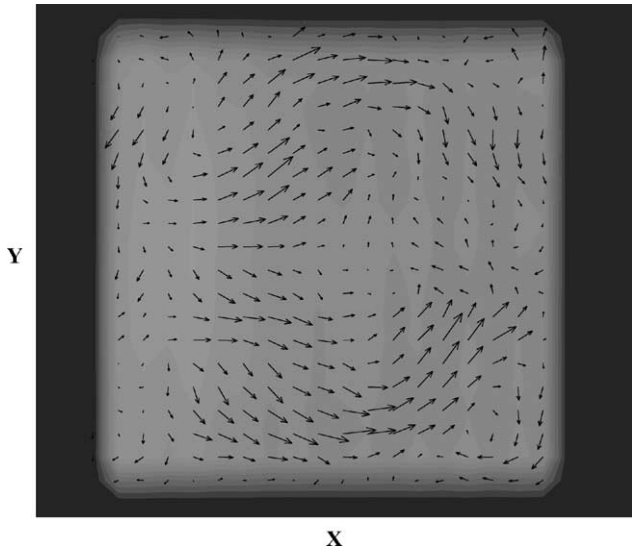

Fig. 8. In-plane velocity vectors in the second passage just downstream of the first bend. Note the presence of the corner vortices. Point spacing is 1.1 mm in X by 1.0 mm in Y.

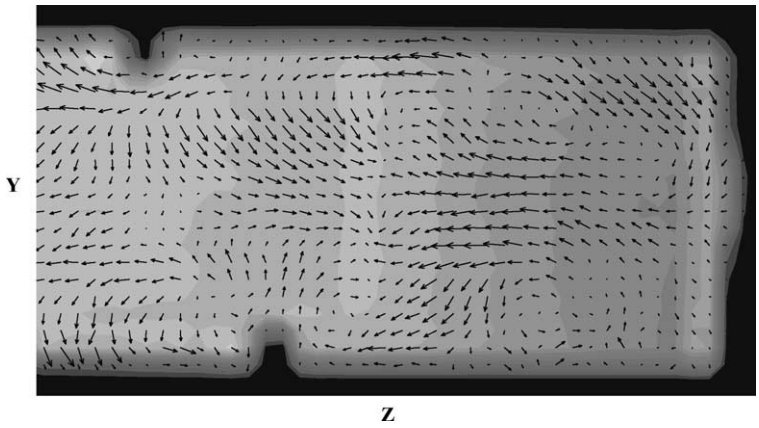

Fig. 9. In-plane velocity vectors in the first bend and second passage along the inside wall. Note the presence of the reverse flow in the middle of the channel to the left of the center of the figure. Flow around turbulators can be seen on the top and bottom of the figure. Point spacing is 1.1 mm in Z by 1.0 mm in Y.

Fig. 9 is a view of the flow in and downstream of the bend in a plane close to the inside sidewall of the bend. The right half of the figure shows flow in the bend where several secondary flow vortices are evident. The left half of the figure shows flow downstream of the bend where the bulk flow direction is right to left. In the middle of the channel, vectors point in the opposite direction indicating the recirculation zone. The reattachment point can be seen where the vectors turn to the left. The flow around the turbulators on the upper and lower walls points to interesting separation and reattachment structures.

3.2. Temperature measurements

Due to the fully developed nature of the flow, only two radial profiles are shown to exhibit the quality of the preliminary temperature measurements. However, it is important to keep in mind that there are velocity and temperature data from an entire 26 cm long three-dimensional volume of the pipe.

Fig. 10(a) shows the radial velocity profile in the fully developed axisymmetric pipe flow experiment. The MRV velocity data are normalized by the centerline velocity and compare well with LDA data in flow at $Re = 17{,}800$ (den Toonder and Nieuwstadt, 1997), a Reynolds number in the middle of the range of Reynolds numbers for the heated and unheated pipe flow. The MRV data are slightly low in the region near the wall where the velocity gradients are highest. This may be due to position misregistration, a common problem with MR data since position is only known with the precision of 1/2 the pixel width. It also may be due to voxel averaging of the velocity in the shear layer, another common problem with MRV.

Fig. 10(b) shows the MRT temperature difference profile. Here, temperature difference is normalized by the predicted temperature difference of 30 °C. The temperature in the region near the wall is low due in part to the slight position error. Also, the temperature in this region is likely to be lower than the isothermal value since the pipe wall is not perfectly adiabatic. Across the rest of the profile, the data show that there is considerable noise in the temperature measurements, about ±20%. Relatively large uncertainty is expected since the source of the temperature signal is a change in resonant frequency of only 0.01 ppm/°C.

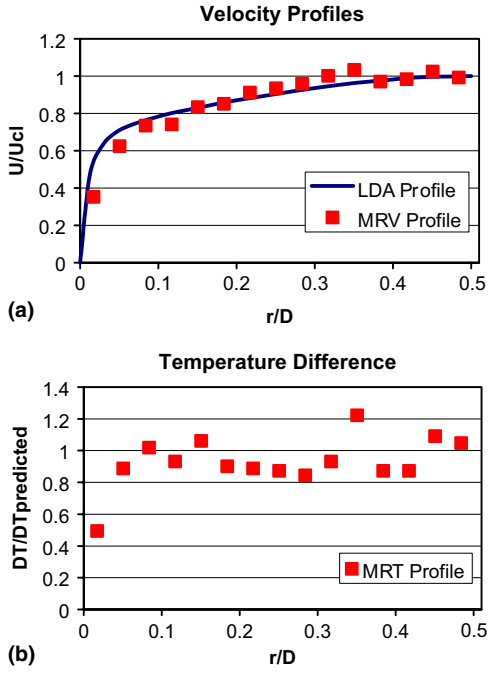

Fig. 10. Velocity and temperature difference profiles measured in heated pipe flow with 4D-MRV/MRT. (a) Mean velocity normalized by centerline velocity in fully developed pipe flow, $Re = 13{,}000$, compared to LDA data at $Re = 17{,}800$ (den Toonder and Nieuwstadt, 1997). (b) Measured temperature difference normalized by the predicted isothermal temperature difference.

4. Discussion

The results illustrate the resolution capabilities of the 4D-MRV technique. Moreover, directly comparing to PIV measurements in the first bend helps to define its quantitative accuracy for measurements in complex highly turbulent flows. The magnitude and vector plots (Figs. 2–4, 8, and 9) show MRV captures the complexity of the flow in the serpentine passage model. From a qualitative aspect, the MRV data clearly show regions of flow characterized by high speed, stagnation, recirculation, shear, etc. This alone makes MRV measurements useful for designers and for comparing to CFD results.

Quantitatively, the MRV vectors agree quite well with the PIV vectors in Fig. 4. The velocities agree within ±10% in magnitude and ±10° in direction over most of the flow in the first bend which is characterized by turbulent fluctuations ranging from 10% to 20% of the passage inlet bulk velocity. MRV errors get higher in the shear layer bounding the separation region where fluctuations reach 50%. This confirms that the MRV technique can be relatively accurate in highly turbulent, accelerating flows.

It is important to put these levels of accuracy into perspective by considering that there is no viable way to measure velocities in many real gas turbine blade internal cooling passages as well as other complex internal flow geometries. Moreover, the flow in and around the bends and turbulators can be especially difficult to predict. The utility of the MRV technique is demonstrated by its ability to capture these flow features with great detail in a short amount of time. These scans took less than 30 min. When coupled with rapid prototyping manufacturing, which is ideal for making MR compatible complex internal passage flow models, the 4D-MRV technique can be a powerful tool for studying these difficult flows in a very short time, on the order of a day. However, it is currently not a mature measurement technique since further work is needed to improve its accuracy. In particular, corrections must be developed for velocity gradient effects and spatial misregistration.

4D-MRT promises to provide similarly detailed data of the entire temperature field in an internal passage. Unfortunately, the experimental design for 4D-MRT is much more complicated since appropriate thermal boundary conditions must be created. In addition, the boundary conditions must be implemented using MR compatible methods. This precludes the use of isothermal copper surfaces and thin film electric heaters. Heated/cooled water jackets are potential devices for heating/cooling the internal flow.

The preliminary 4D-MRV/MRT results in the heated pipe flow are encouraging and point to the potential of this method for measuring the complete mean velocity and thermal field in complex 3D flow geometries. The results also underscore the need for more development. In particular, the signal to noise ratio for temperature measurements using the 4D-MRV technique is quite low. Improving the signal will likely require the adoption of a different sequence or the development of a new sequence. One possibility is to use a sequence with flow compensation. In steady non-accelerating flows, such a sequence would measure temperature without the fluid motion effects. However, in these complex internal flows, higher order accelerations will produce additional errors that must be considered.

This basic experiment pointed out additional problems to be overcome. One of which is that the viscosity of water is a strong function of temperature. In using the MRV/MRT technique, it will be necessary to design experiments in which the flow fields remain similar for considerably different Reynolds numbers. Depending on the flow of interest, this may be as simple as insuring that both the heated and unheated flows are non-transitional.

Finally, the 4D-MRV technique provides very detailed three-dimensional data ideal for comparing to CFD. Since CFD relies on models that have difficulty in regions of complex flow, the 4D-MRV data are quite useful as validation data.

5. Conclusions

We have applied an experimental technique called 4D-MRV to the study of flow in a model of a gas turbine blade internal cooling geometry with four serpentine passages. Three-component mean velocities were obtained for a Reynolds number of 10,000 based on mean bulk velocity and passage height. The 4D-MRV measurements were evaluated for accuracy using PIV measurements in a 180° bend. This region of the flow is characterized by strong turning and velocity fluctuations ranging from 10% to 50% of the inlet mean bulk velocity. Velocity magnitudes are accurate to within ±10% and velocity vector angles accurate to within ±10° for most of the flow. The density of velocity measurements makes these data sets particularly useful for comparison with CFD calculations. The full dataset is available from the authors on their website.

We have also completed a preliminary experiment using a 4D-MRV/MRT technique for measuring mean velocity and temperature in heated fully developed pipe flow. These measurements provided mean velocity vectors and temperatures in an entire 26 cm long three-dimensional volume inside the pipe. Velocity measurements agreed well with data in the literature. Temperature data were accurate to ±20%, an encouraging result that points to the great potential of this method for making full-field temperature measurements in heated 3D flow geometries.

Acknowledgments

Financial support was provided by the Department of Energy as part of the ASCI program at Stanford University. Use of the facilities at the Richard M. Lucas Center for Magnetic Resonance Spectroscopy and Imaging is gratefully acknowledged. The flow models were manufactured in the W.M. Keck Border Biomedical Manufacturing and Engineering Laboratory at UTEP with assistance from Francisco Medina. Manufacturing of the flow models and the PIV measurements were performed at UTEP and funded, in part, through Grant #11804 from the W.M. Keck Foundation and the endowed Mr. and Mrs. Macintosh Murchison Chair I in Engineering.

References

Bertsch, F., Mattner, J., Stehling, M.K., Muller-Lisse, U., Peller, M., Loeffler, R., Weber, J., Messmer, K., Wilmanns, W., Issels, R., Reiser, M., 1998. Non-invasive temperature mapping using MRI: comparison of two methods based on chemical shift and T1-relaxation. Magn. Reson. Imaging 16 (4), 393–404.

Bogren, H.G., Buonocore, M.H., 1999. 4D magnetic resonance velocity mapping of blood flow patterns in the aorta in young vs. elderly normal subjects. J. Magn. Reson. Imaging 10, 861–869.

Cline, H.E., Hynynen, K., Schneider, E., Hardy, C.J., Maier, S.E., Watkins, R.D., Jolesz, F.A., 1996. Simultaneous magnetic resonance phase and magnitude temperature maps in muscle. Magn. Reson. Med. 35 (3), 309–315.

den Toonder, J.M.J., Nieuwstadt, F.T.M., 1997. Reynolds number effects in turbulent pipe flow for low to moderate *Re*. Phys. Fluids 9, 3398–3409.

Diedrich, C.J., Stafford, R.J., Price, R.E, Nau, W.H., Tyreus, P.D., Rivera, B., Shomer, D., Olsson, L., Hazle, J., 2001. Minimally invasive ultrasound thermal therapy with MR thermal monitoring and guidance. Proc. SPIE—Int. Soc. Opt. Eng. 4247, 166–170.

Ebbers, T., Wigstrom, L., Bolger, A.F., Engvall, J., Karlsson, M., 2001. Estimation of relative cardiovascular pressures using time-resolved three-dimensional phase contrast MRI. Magn. Reson. Med. 45, 872–879.

Elkins, C., Eaton, J.K., Markl, M., Pelc, N., 2003. 4D magnetic resonance velocimetry for mean velocity measurements in complex turbulent flows. Exp. Fluids 34, 494–503.

Fukushima, E., 1999. Nuclear magnetic resonance as a tool to study flow. Ann. Rev. Fluid Mech. 31, 95–123.

Gach, H.M., Lowe, I.J., 2000. Measuring flow reattachment lengths downstream of a stenosis using MRI. J. Magn. Reson. Imaging 12, 939–948.

Gatenby, J.C., Gore, J.C., 1996. Echo-planar-imaging studies of turbulent flow. J. Magn. Reson. A 121, 193–200.

Haacke, M., Brown, R., Thompson, M., Venkatesan, R., 1999. Magnetic Resonance Imaging. Wiley-Liss, New York.

Kozerke, S., Hasenkam, J.M., Pedersen, E.M., Boesiger, P., 2001. Visualization of flow patterns distal to aortic valve prostheses in humans using a fast approach for cine 3D velocity mapping. J. Magn. Reson. Imaging 13, 690–698.

Ku, D.N., Biancheri, C.L., Pettigrew, R.I., Peifer, J.W., Markou, C.P., Engels, H., 1990. Evaluation of magnetic resonance velocimetry for steady flow. J. Biomech. Eng. 112, 464–472.

Li, T.Q., Seymour, J.D., Powell, R.L., McCarthy, K.L., Odberg, L., McCarthy, M.J., 1994. Turbulent pipe flow studied by time-averaged NMR imaging: measurements of velocity profile and turbulent intensity. Magn. Reson. Imaging 12, 923–934.

Mantle, M.D., Sederman, A.J., 2003. Dynamic MRI in chemical process and reaction engineering. Prog. Nucl. Magn. Reson. Spectrosc. 43, 3–60.

Markl, M., Chan, F.P., Alley, M.T., Wedding, K.L., Draney, M.T., Elkins, C.J., Parker, D.W., Wicker, R., Taylor, C.A., Herfkens, R.J., Pelc, N.J., 2002. Time resolved three dimensional phase contrast MRI (4D-Flow). J. Magn. Reson. Imaging 17, 499–506.

Nott, K.P., Hall, L.D., 1999. Advances in temperature validation of foods. Trends Food Sci. Technol. 10, 366–374.

Ogawa, K., Tobo, M., Iriguchi, N., Hirai, S., Okazaki, K., 2000. Simultaneous measurement of temperature and velocity maps by inversion recovery tagging method. Magn. Reson. Imaging 18, 209–216.

Oshinski, J.N., Ku, D.N., Pettigrew, R.I., 1995. Turbulent fluctuation velocity: the most significant determinant of signal loss in stenotic vessels. Magn. Reson. Med. 33, 193–199.

Seigel, J.M., Oshinski, J.N., Pettigrew, R.I., Ku, D.N., 1996. The accuracy of magnetic resonance phase velocity measurements in stenotic flow. J. Biomech. 29, 1665–1672.

Stark, D., Bradley, W., 1999. Magnetic Resonance Imaging. Mosby-Year Book, St. Louis.

Sun, L., Hall, D., 2001. An experimental solution of the Graetz problem in heat exchangers. Int. Commun. Heat Mass Transfer 28 (4), 461–466.

von Schulthess, G., Hennig, J., 1998. Functional Imaging. Lippincott-Raven, Philadelphia, pp. 261–390.